



# Enhancing mechanical performance of 3D printable PMMA resin through strategic incorporation of SS 316 L nanoparticles for dental applications

Upender Punia<sup>1</sup> · Ramesh Kumar Garg<sup>1</sup>

Received: 9 October 2023 / Accepted: 23 July 2024

© The Author(s), under exclusive licence to Springer-Verlag France SAS, part of Springer Nature 2024

## Abstract

In the present study, a nano composite PMMA was prepared with the help of hot plate magnetic stirring and probe sonication at different loading conditions of reinforcement material SS 316 L. In order to study the effect of independent factors (the amount of reinforcement material, stirring speed, and sonication time) on response variables, the central composite experimental design of response surface methodology was utilized. The microstructure (surface morphology and topography) was analysed by SEM and AFM, resulting in homogeneous dispersion of nano particles. The analysis of the RSM results indicated that the experimental data were most accurately represented by a quadratic polynomial model, with regression coefficient values exceeding 0.960 for all the responses. The optimum preparation conditions for PMMA nano-composite to achieve the best specific wear rate and compression strength were found to be as follows: the addition of 1.16% (w/w) of reinforcement material SS 316 L, a stirring speed of 1200 rpm, and a sonication time of 29.6 min. The results of this study hold great significance in the fabrication process of long-term provisional dental crowns and bridges.

## Highlights

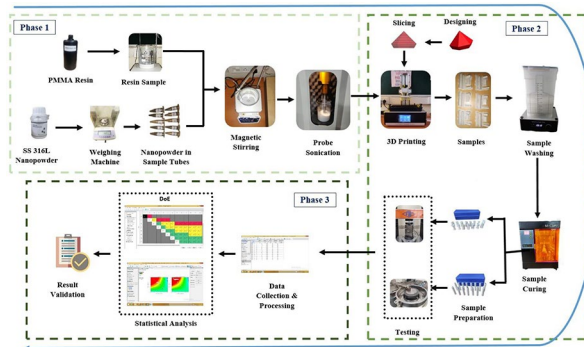
- A nano composite was prepared using SS 316 nanoparticles as reinforcement material.
- The effect of independent process parameter was investigated using RSM model.
- The compression strength and wear rate of nanocomposite were studied.
- The microstructure was visualised by using SEM and AFM images.
- The novel fabricated 3D printable nanocomposites was found more effective.

---

✉ Upender Punia  
punia899195@gmail.com

<sup>1</sup> Department of mechanical engineering, DCRUST, Murthal, Sonapat, Haryana 131039, India

## Graphical Abstract



The process flow chart consists of 3 Phases. **Phase 1:** Preparation of nanocomposite of PMMA resin and SS 316 L nanopowder using magnetic stirring and probe sonication. **Phase 2:** Fabrication of nanocomposite using resin 3D printer and investigation of mechanical properties (compression strength and wear rate) and microstructure (SEM and AFM images). **Phase 3:** Result analysis and validation using response surface methodology

**Keywords** Composite materials · Reinforcement · Additive manufacturing · Mechanical properties · Response surface methodology

### Abbreviations

PMMA	Poly methyl methacrylate
SS 316L	Stainless steel with grade 316 L
RSM	Response surface methodology
SEM	Scanning electron microscopy
AFM	Atomic force microscopy
w/w	Weight by weight
rpm	Revolution per minute
3d Printing	Three-dimensional printing
UV	Ultraviolet

## 1 Introduction

Computer-aided design and manufacturing (CAD/CAM) technologies have been extensively utilized in various industries since the 1980s [1]. Particularly, the advent of 3D technologies has brought about significant advancements across sectors such as automotive, medical, defense, etc. In the realm of medical applications, traditional techniques have increasingly been replaced by digital fabrication and design processes [2, 3]. One particularly noteworthy tool that has gained popularity is 3D printing. This technique has the ability to create hollow, small, intricate, and complex models with remarkable precision and accuracy, all while remaining cost-effective [4]. Resin printing stands out as a highly effective technology among all 3D printing processes, particularly when it comes to producing small size models like provisional tooth crowns, bridges, occlusal splints, and denture bases with exceptional accuracy and precision [5–7].

The provisional restoration is very important in ensuring the safety of the surgical area, enhancing aesthetics, and providing functional benefits in fixed restorations [8, 9]. Typically, resin-based composites combined with coupling agents are used for fabricating these provisional restorations. But the functional environment creates significant challenges for these restorations to have excellent capabilities to fulfil their intended functions [10]. Researchers have been dedicated to improving the mechanical, physical, and chemical properties of provisional restorations by modifying the resin matrix and refining fabrication techniques [11]. These efforts aim to enhance the overall performance and durability of provisional restorations [12]. However, several of these alterations had unfavourable side effects that reduced the material's performance, such as raising porosity, lowering biological compatibility, and restricting cure depth and etc. [13]. PMMA has many good characteristics as a biomaterial regarding its cost, aesthetics, and easy fabrication [14], but it has some drawbacks which arise while fabricating prosthodontic restoration, such as presence of residual monomers, dimensional instability/shrinkage, low compression and impact strength, thermal conductivity and expansion, crazing, discoloration, and porosity [15]. These drawbacks raise problems of dental fracture and poor bending strength. To overcome these drawbacks, PMMA is reinforced with some nano-fillers/micro-filler of fibres/metals/thermoplastics/ antimicrobial to achieve the desired properties [16]. The addition of a small number of metals and ceramics nanoparticles drastically affects PMMA material's properties [17]. In recent studies, the researchers investigated the various properties, i.e., thermal, mechanical,

morphological, micro structural, and biological, of reinforced PMMA and concluded the improvement [18]. There is also the effect of surface area, dispersion in the matrix, and type of nanoparticles on the reinforced material [19–21]. The addition of ceramic and metallic nanoparticles is found to be the best reinforcement for mechanical properties. The metallic reinforcement also improves the thermal properties resulting in the food temperature judgment [22, 23]. The addition of carbon nanotubes in PMMA resulted in better mechanical and electrical properties, and multiwall CNTs showed better results than single-wall CNTs [24].

Maram et al. added nanoparticles of SiO<sub>2</sub> and ZrO<sub>2</sub> in 3D-printable provisional dental resin (PMMA) and found that the addition of nanoparticles increased the hardness without compromising the surface roughness, flexural strength with 0° orientation and thermal cycling did not significantly affected the composite resins [25, 26]. The addition of lanthanum-ion-coordinated multidimensional nanoceramic reinforcements of modified ZrO<sub>2</sub> and BNNs improved the antifriction and wear resistance properties of 3D printed acrylic matrix composites [27]. Aati et al. added functionalized ZrO<sub>2</sub> nanoparticles in 3D printed acrylate resin and revealed that Vickers hardness flexural strength improves with filler content [28]. SS 316 L is a medical grade of stainless steel, which is having low carbon content and high corrosion resistance, offers numerous advantages in the fabrication of dental crowns, particularly for paediatric dentistry [29, 30]. High strength and durability are significant advantages of employing stainless steel 316 L in dental crowns. One of the major advantage of SS 316 L in dental crowns is its long term durability and high strength. It can withstand biting forces and provides long-lasting performance. Additionally, stainless steel crowns are highly resistant to corrosion and cost-effective compared to other crown materials [31, 32]. However, stainless steel crowns are not typically recommended for permanent use in adult dentistry due to aesthetic concerns due to metallic appearance. So, it is especially used for temporary crowns or in situations where long-term durability is not the primary concern [33, 34].

The goal of this present research is to generate a new 3D printable provisional dental restoration based resin material modified with nano-fillers of medical grade stainless steel and investigate the impact of stirring speed and sonication time at various loading condition of SS 316 L nanoparticles. To achieve this goal, different stirring speeds and sonication time were chosen to produce different PMMA based nano composites. The work is novel as the SS 316 L has never been added

in nanoparticle form in PMMA resin to develop 316 L/PMMA nanocomposite in 3D printing applications in the existing literature. The results of this investigation were analysed using ANOVA testing and discussions from existing literature.

## 2 Materials and methods

### 2.1 Materials

The dental resin material, PMMA (poly methyl methacrylate), was purchased from 3 Idea Technology LLP (Mumbai, Maharashtra, India). It has a viscosity ranging from 1.15 to 1.20 g/cm<sup>2</sup> and comes in a white color. The nano powder used was stainless steel 316 L, purchased from Vedayukt India Private Limited (Jamshedpur, Jharkhand, India). This powder has a particle size range of 20–40 nm and a purity level of 99%. The ethanol and Isopropyl alcohol ((CH<sub>3</sub>)<sub>2</sub>-CH-OH) with purity 99.9% was purchased from Science Sales (Sonipat, Haryana, India). All the materials that were obtained, were used without any alteration and surface modification.

### 2.2 Design of experimentation

The Design Expert<sup>13</sup> software was used for design of experimentation. This software can effectively explore various experimental designs and optimize their outcomes by analyzing the impact of different factors on multiple responses. The software provides a comprehensive suite of tools to enhance the efficiency and effectiveness of experimental design processes. Three factors were taken based on the literature, and their levels were decided on the basis of pilot experimentation and literature [35–37]. The three factors and their levels are represented in Table 1. The central composite design (CCD) was chosen in response surface methodology (RSM) study due to its higher order model capability, better efficiency in estimating quadratic terms and literature support [38–40]. A total of 15 sets of combination of experiments were obtained from central composite design taking face-centered alpha, single replicate of factorial points, single replicate of star point, and five center points.

### 2.3 Preparation of nanocomposite

The fabrication process of the nano composite involved incorporating nanopowder at various concentrations (0.5% (w/w), 1.0% (w/w), and 1.5% (w/w)) under specific working

**Table 1** Factors and their levels in design of experimentation

S. No.	Factor	Unit	No. of Level	Level 1	Level 2	Level 3
1	SS 316 L	% (w/w)	3	0.5	1	1.5
2	Stirring speed	rpm	3	800	1100	1400
3	Sonication time	minute	3	10	20	30

parameters using a hot plate magnetic stirrer and a probe sonicator [41]. The nanopowder was first cleaned in ethanol to ensure purity. For accurate measurement, a weighing scale with a least count of 0.0001 g was utilized to weigh the nanopowder samples. Subsequently, the dispersion process commenced by gradually adding the nanopowder into the resin material while subjecting it to hot plate magnetic stirring for a duration of 120 min. This stirring process facilitated the uniform distribution and incorporation of the nanopowder within the resin matrix. After the stirring phase, the sample underwent sonication at a frequency of 20 kHz using a probe sonicator [28, 42]. This ultrasonic treatment further aided in the dispersion and homogenization of the nanoparticles, promoting their homogeneous distribution throughout the resin material. By following this methodology, the nano composite was synthesized, ensuring an efficient dispersion of the nanopowder within the resin matrix, which is crucial for obtaining desirable material properties and performance.

## 2.4 Design and fabrication of specimen

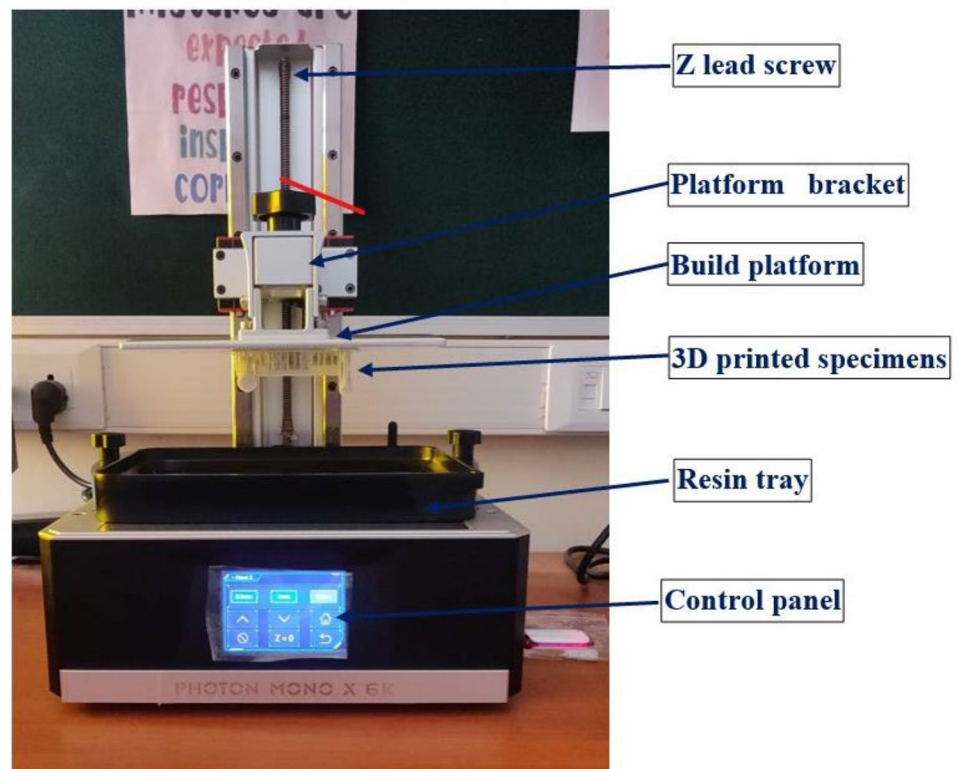
The geometries and sizes of all the specimens were designed as per ASTM standards using solid works software. To prepare the models for 3D printing, Anycubic Photon Workshop V2.2.16 software is used to slice the designs into printable layers. For the fabrication process, the ANYCUBIC Photon

Mono X 6 K 3D printer was used, which is shown in Fig. 1. The printing parameters were maintained consistently throughout the printing process, with an exposure time of 4 s, a bottom exposure time of 40 s, a layer height of 30 microns, and a light off time of 0.5 s. These parameters were crucial in ensuring accurate and reliable prints. Once the printing was complete, the printed specimens were carefully removed from the build plate, and proceeded to remove any support material. The specimens were washed in an IPA (Isopropyl Alcohol) solution for 10 min. This step helped in removing excessive resins and ensuring the cleanliness of the printed parts. Then the samples were left to cure for 40 min in a curing unit.

## 2.5 Compression test

The compression test was performed on the cylindrical specimens fabricated as per ASTM D695 standards, whose dimensions are 12.7 mm × 12.7 mm × 25.4 mm. Compression strength was measured by placing the specimen between two plates made of hardened steel using a universal testing machine (FIE UNITEK 94100; shown in Fig. 2a). The axial compressive force was exerted on the specimen with a test speed of 5 mm/min.

**Fig. 1** Depicts a resin 3D printer & its components during the fabrication process. Platform bracket serves as a fixture for build plate; Build platform, also known as the build plate on which the product is fabricated; Specimens for evaluation of mechanical properties; Resin tray for holding the resin material; and control panel responsible for managing and controlling the process and provides real-time data



## 2.6 Wear rate test

ASTM G99 standards were used to perform wear test on the fabricated cylindrical sample of 8 mm diameter and 30 mm length. The friction force, wear rate, and friction coefficient were determined using the Pin-on-Disc Wear testing machine (DUCOM Tr-20LE; shown in Fig. 2b). The sample was inserted in place of the pin, and a disc of hardened EN31 material was used to find out the wear in composite material. Each specimen was traveled against the rotating disc for 5 min at 500 rpm, keeping the track diameter 7 cm with a load of 20kN at ambient temperature conditions.

While the wear results were described in volume loss per meter distance traveled with or without taking the impact of load. The specific wear rate in terms of  $m^3/Nm$  was calculated from Eq. (1) considering the effect of dependent load, whereas the wear rate in terms of  $m^3/m$  was calculated from Eq. (2) using independent load.

$$\begin{aligned} \text{Specific Wear rate (Ws)} \\ = \frac{\text{wear volume loss}}{\text{sliding distance} \times \text{load applied}} m^3/Nm \end{aligned} \quad (1)$$

$$\begin{aligned} \text{Wear rate (W)} \\ = \frac{\text{wear volume loss}}{\text{sliding distance}} m^3/m \end{aligned} \quad (2)$$

where;  $W_s = \frac{m_i - m_f}{L.F.\rho}$ ; where F- Load applied,  $\rho$  – Density, L – Sliding distance,  $m_i$  – initial mass (before testing),  $m_f$  – final mass (after testing).

## 2.7 Microscopic characterization

The study involved the examination of both modified and unmodified 3D printed specimens using a scanning electron microscope (JOEL: JSM 6610LV) to investigate the surface morphology of the fractured specimens. First of all, samples were placed on the fixtures for stable mounting. Then, a gold-palladium coating was applied to their surfaces using a Gold sputter coater model JEC 300. This coating is necessary to make the specimen surfaces conductive, allowing for effective imaging using the SEM. Once coated, the specimens were transferred to an evacuated chamber within the SEM for microscopic characterization. During the imaging processing, the SEM was operated at a voltage of 20 kV, a working distance of 12 mm, and various magnifications to get the best image results. To analyze the distribution of SS 316 L nano-fillers and surface topography, an atomic force microscope (Bruker Dimension Edge) was used. High-resolution images were captured using a scanning rate of 20–40  $\mu m/s$  and a set point amplitude of 30 mV. The images were taken with different scan sizes in order to obtain the most detailed microscopic structures. A total of  $256 \times 256$  sample lines were used for each image. Three-dimensional images were reconstructed using Nanoscope Analysis 1.5 software to further analyze the surface characteristics by utilizing the appropriate and precise insights.

## 2.8 Statistical analysis

The data was collected from experimental results and statistically analyzed using Design-Expert 13. Box-Wilson or Center composite design was used to tabulate the combination of input parameters at their different levels. Various statistical characteristics, such as lack of fit, coefficient of

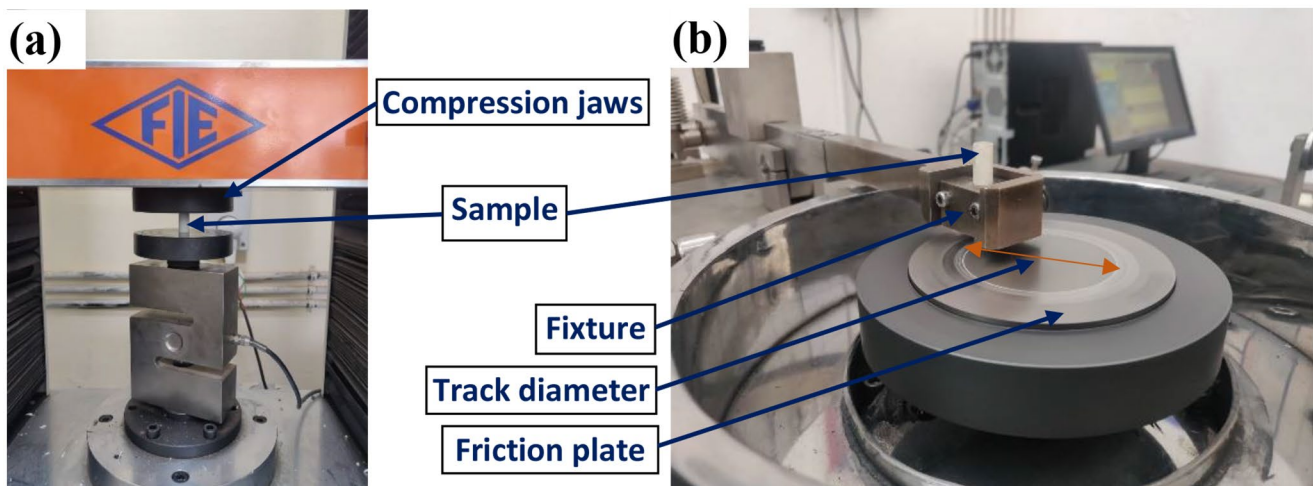


**Fig. 2** Testing setup for (a) Compression strength on UTM in which the specimens was placed between the compression dies; and (b) Wear rate on Pin-on-disc apparatus in which the sample specimen was hold by a fixture and rubs against a friction plate made of metallic alloy EN31

variation, and estimated and modified numerous correlation coefficients, were carefully evaluated among various polynomial models to determine the most suitable model with a statistical significance of  $p \leq 0.05$ . To understand the effect of input factors on responses, one factor, interaction graphs, and 3D response graphs were generated using Design Expert<sup>13</sup> software.

### 3 Results and discussion

In the experimental phase of this study, the compression tests and pin-on-disc wear tests were conducted on composite resins commonly used in dentistry. These composite resins were prepared by dispersing nano-fillers with the resin in varying proportions and employing different stirring speeds and sonication times during the preparation process. In compliance with ASTM prerequisites, the composite resin specimens were made using the ANYCUBIC Photon Mono X 6 K resin 3D printer. To evaluate their compression behavior, the stress-strain and load-deflection curves and various other characteristics were examined that provided insight into the samples' performance during testing. We were able to compute the elastic modulus, proportionality limit, and yield strength by examining the stress-strain data collected from compression testing. Meanwhile, the data collected during the pin-on-disc wear test was utilized to calculate the wear rate, frictional forces, and coefficient of friction.

#### 3.1 Compression tests

The compressive strength of the 3D fabricated test samples was evaluated using a universal testing machine (UTM). A total of 16 readings (1 unmodified and 15 modified samples) were obtained, as illustrated in Table 2, to create a test configuration for determining the compressive strength of 3D fabricated test pieces with varying composition and processing parameters. These parameters include the amount of nano-filler, stirring speed, and sonication time. The test pieces underwent testing on the UNITEK 94,100 UTM, as illustrated in Fig. 2(a). The relationship between the input factors and the compression strength is expressed by a quadratic equation that incorporates two-factor interaction, as depicted in Eq. (3).

$$\begin{aligned} \text{Compression strength} = & 63.1013 \\ & + 139.853A + 0.0233007B + 0.22598C \\ & + 0.015AB + 0.25AC + 0.0000833BC \\ & - 77.1765A^2 - 0.0000143B^2 + 0.00294C^2 \end{aligned} \quad (3)$$

where, A – reinforcement material, B – stirring speed, C – sonication time.

The analysis revealed that the samples had varying compressive strengths depending on the processing parameters. For example, sample (Run 14) with 1% (w/w) reinforcement, a stirring speed of 1400 rpm, and a sonication time of 30 min exhibited a compressive strength of 0.165 kN/mm<sup>2</sup>, as depicted in Fig. 3. On the other hand, sample (Run 6) with 0.5% (w/w) reinforcement, a stirring speed of 800 rpm, and a sonication time of 10 min had the minimum compressive

**Table 2** Responses of compression strength and specific wear rate

Std	Run	Factor 1 A: Reinforcement Material (% (w/w))	Factor 2 B: Stirring Speed (rpm)	Factor 3 C: Sonication time (min)	Response 1 Compression Strength (MPa)	Response 2 Specific Wear Rate (mm <sup>3</sup> /Nm)
		Unmodified			118	0.728
3	1	0.5	1400	30	140	0.613
7	2	1	800	20	157	0.564
15	3	1	1100	20	160	0.561
6	4	1.5	1100	20	145	0.551
1	5	1.5	1400	10	142	0.542
4	6	0.5	800	10	133	0.634
13	7	1	1100	20	161	0.552
12	8	1	1100	20	162	0.558
5	9	0.5	1100	20	138	0.628
14	10	1	1100	20	161	0.550
11	11	1	1100	20	159	0.563
2	12	1.5	800	30	144	0.532
9	13	1	1100	10	156	0.564
10	14	1	1100	30	165	0.541
8	15	1	1400	20	162	0.557

strength of  $0.133 \text{ kN/mm}^2$ . In contrast, sample (Run 12), which consists of 1.5% (w/w) reinforcement, was prepared using an 800 rpm stirring speed and 30 min of sonication time and exhibited a compressive strength of  $0.144 \text{ kN/mm}^2$ .

### 3.2 Wear behavior

The wear samples were subjected to testing using the DUCOM pin-on-disc wear testing machine. All parameters, such as speed, running time, radius, load, and temperature, were kept constant for each sample. The machine provided experimental data for the friction force and wear. The wear results for each specimen were determined by measuring the initial mass before testing and the final mass after testing for all combinations. Each specimen exhibited varied values depending on the factors involved, and the absolute computed value was recorded as the response for each test run, as illustrated in Table 2. The relationship between the frictional forces v/s time, wear v/s time, and coefficient of friction v/s time is depicted in Fig. 4. In the plotted graphs as represented in Fig. 4 (a) and (b), it seems that the friction force and coefficient of friction initially increase rapidly and then stabilize. This pattern suggests that the fabricated samples have a consistent surface quality. The consistent friction force and coefficient of friction indicate that the

materials used in the samples have consistent properties throughout. On the other hand, the gradual increase in wear and the presence of fluctuations in the graph depicted in Fig. 4 (c) suggest the incorporation of nano fillers in the samples. The variation in wear and the presence of fluctuations in the graphs may indicate the non-uniform distribution or arrangement of these nano fillers within the samples. The frictional force and coefficient of friction increase rapidly at its initial stage and then keep almost constant for the complete process. The connection between the input factors and the specific wear rate is expressed through a quadratic equation incorporating two-factor interaction, as denoted in Eq. (4).

$$\begin{aligned} \text{Specific wear rate} = & 0.773199 - 0.283676A \\ & - 0.000034B + 0.000199C - 0.000025AB \\ & - 0.00015AC + 0.00000158BC + 0.118A^2 \\ & + 7.189 \times 10^{-9} B^2 - 0.0000735C^2 \end{aligned} \quad (4)$$

### 3.3 Microstructure

The SEM images of the fractured specimens provide valuable insights into the surface morphology and composition of the reinforced and parent dental resin. In Fig. 5(a), the

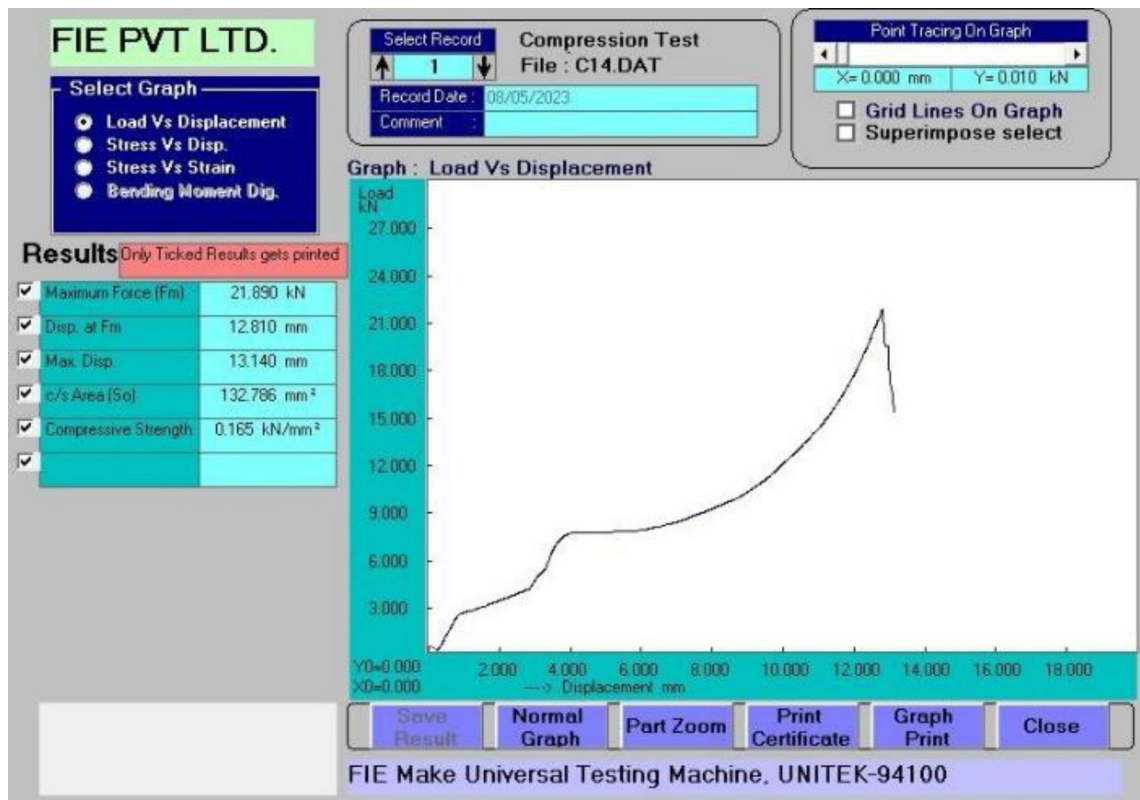
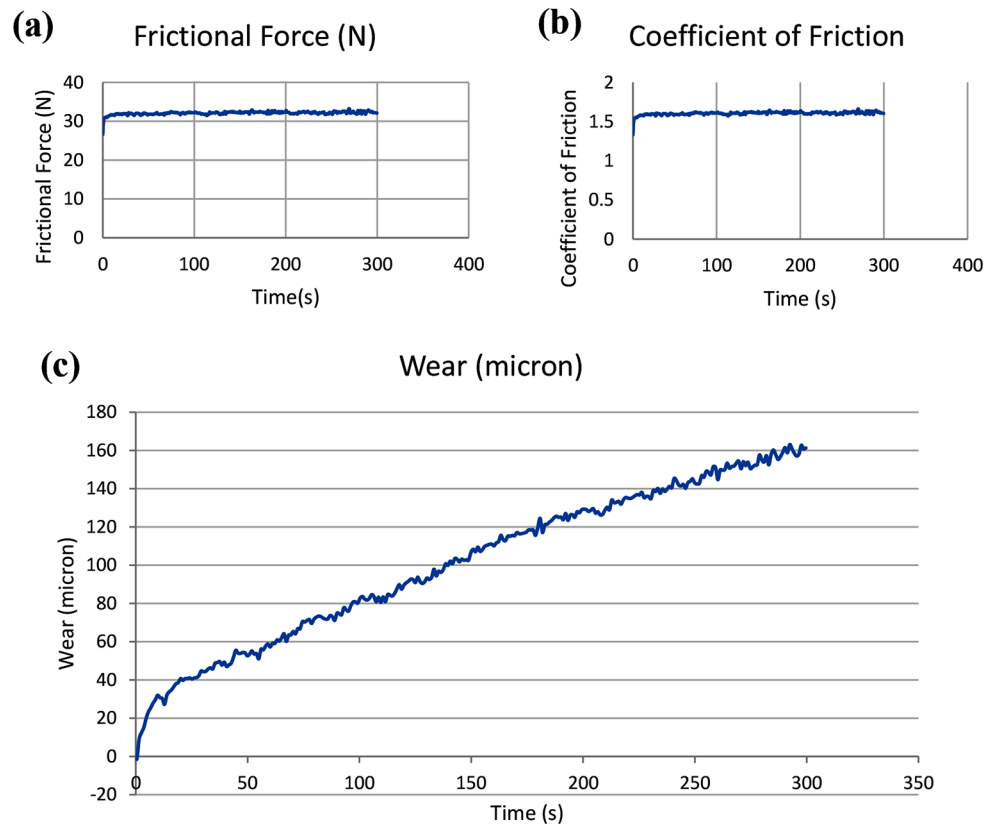


Fig. 3 Graphical representation of load versus displacement of compression test (Sample 14)

**Fig. 4** Graphical representation of (a) Frictional force v/s time & (b) Coefficient of friction v/s time exhibiting almost constant behavior of friction and coefficient of friction with time with minor fluctuations; and (c) Wear versus time representing the gradual increase of wear over time with some up and downs attributing to the presence of nanoparticles



smooth surface of the unmodified resin indicates a fracturing behavior. The white surface depicted in the images represents the edges present at the surface. In Fig. 5(b), the presence of SS 316 L nanoparticles can be observed at certain points. These nanoparticles appear spherical in shape, indicating that they are evenly dispersed within the resin matrix during the fabrication process. In Fig. 5(c), the addition of 1% SS 316 L results in the homogeneous distribution of nanoparticles within the resin matrix. The pattern of roughness observed in the SEM images for the 0.5% and 1% additions of SS 316 L nano-fillers is similar to that of the parent dental material. However, as the amount of reinforcement material is increased from 1 to 1.5%, a greater number of cracks becomes visible on the surface. Additionally, the nanoparticles are observed to be positioned closer to each other, and some of them have fused together. The surface roughness appears to enhance with the rise in the amount of reinforcement material, as observed in Fig. 5. The images (e) and (f) in Fig. 5 indeed show crack lines present at multiple places on the surface of the fractured specimen, indicating the occurrence of stress concentration and potential failure points. The agglomeration of SS 316 L nanoparticles can be observed at these crack sites, suggesting that the nanoparticles may contribute to the initiation or propagation of cracks. However, it is important to note that there is no evident presence of irregular and heavy voids in

the images, suggesting a reasonably homogeneous dispersion of the nanoparticles inside the resin matrix.

The atomic force microscope provides three-dimensional images that depict the distribution of materials on the surface of the base resin and its interaction with SS 316 L nanoparticles under different loading conditions (Fig. 6a-d). Figure 6(a) illustrates the smooth surface of the unmodified base resin. In the images of the base resin combined with varying concentrations of SS 316 L, distinct peaks of different magnitudes can be observed. The surface pattern appears to be similar for the 0.5% and 1.5% loading conditions. However, in the case of the 1% loading condition, irregular peaks are noticeable. The dispersion of nanoparticles seems to be evenly distributed across the surface (as seen in Fig. 6b and d). The highest peak observed for the base resin is 42 nm, whereas for the addition of 1.5% nanoparticles, the highest peak measures 103 nm. As the concentration of nanoparticles increases, there is a corresponding increase in surface roughness was observed.

### 3.4 Validation of model

Response Surface Methodology (RSM) is a powerful statistical technique used in experimental design, analysis, and optimization. By fitting the data to this mathematical model, RSM helps to gain insights into the interactions



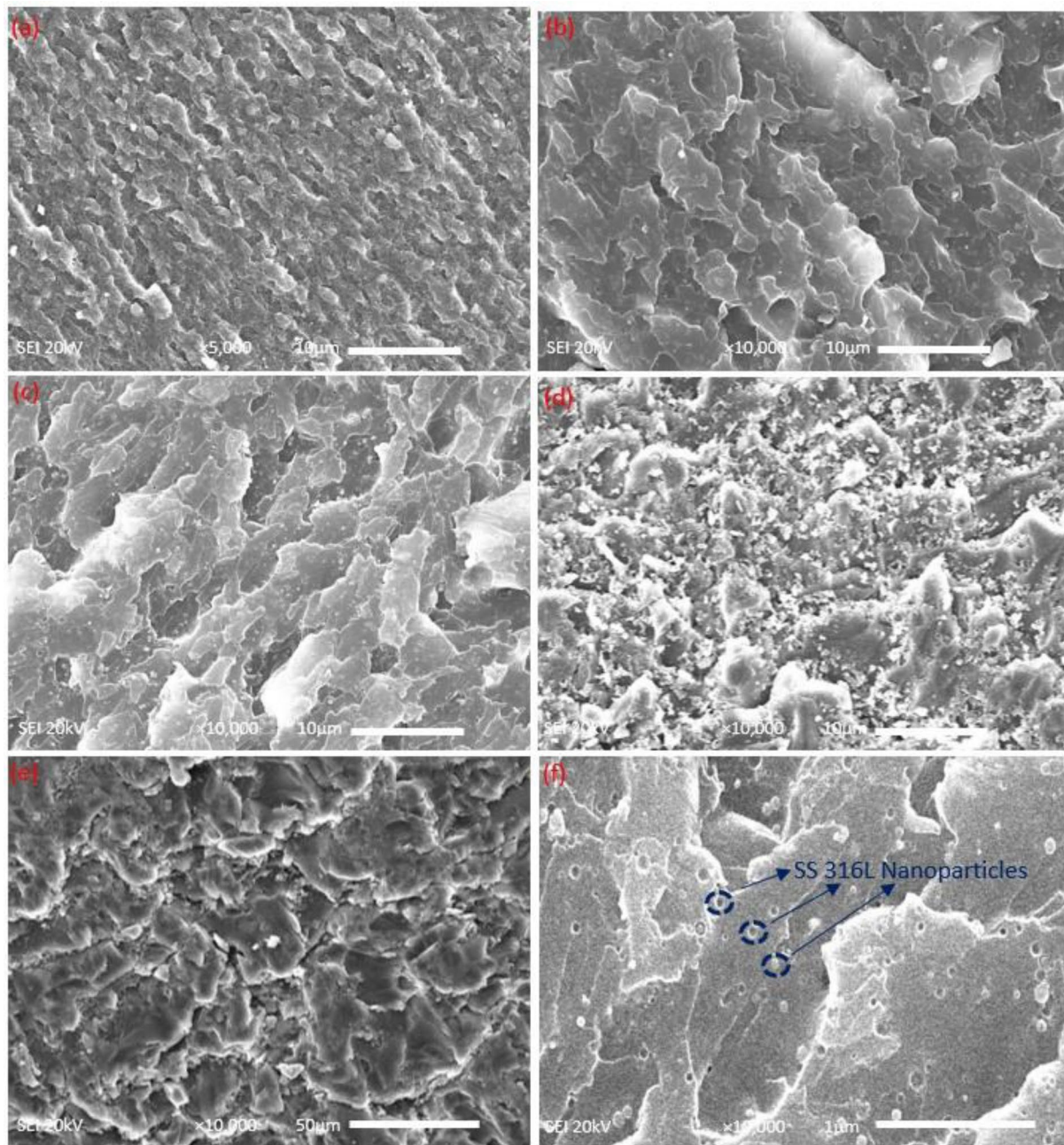


**Fig. 5** illustrates the SEM images of distributed SS 316 L nano-fillers and fractured surfaces (a) Parent dental resin, (b) parent resin added with 0.5%, (c) added with 1%, and (d) added with 1.5% SS 316 L

nano-filler, (e) fracture lines represented at multiple places on the surface, and (f) uniformly distributed nanoparticles

among multiple variables and identify the optimum settings that maximize or minimize the response. The key principle behind RSM is the assumption that the response variable can be approximated by a polynomial function of the input variables. The effect of independent variable reinforcement material (A), stirring speed (B), and sonication time (C) is represented in Table 2. The regression equations of the responses are computed from the experimental data in

quadratic form with two factor interaction, as mentioned in Eqs. (3) and (4).

Based on the ANOVA results, it was found that the experimental data can be effectively represented by a quadratic polynomial model. The coefficient of determination ( $R^2$ ) values for compression strength (R1) and specific wear rate (R2) were determined to be 0.9907 and 0.9685 respectively, as shown in Table 3. Furthermore, the lack of fit was not statistically significant ( $p \leq 0.05$ ) compared to pure error for all

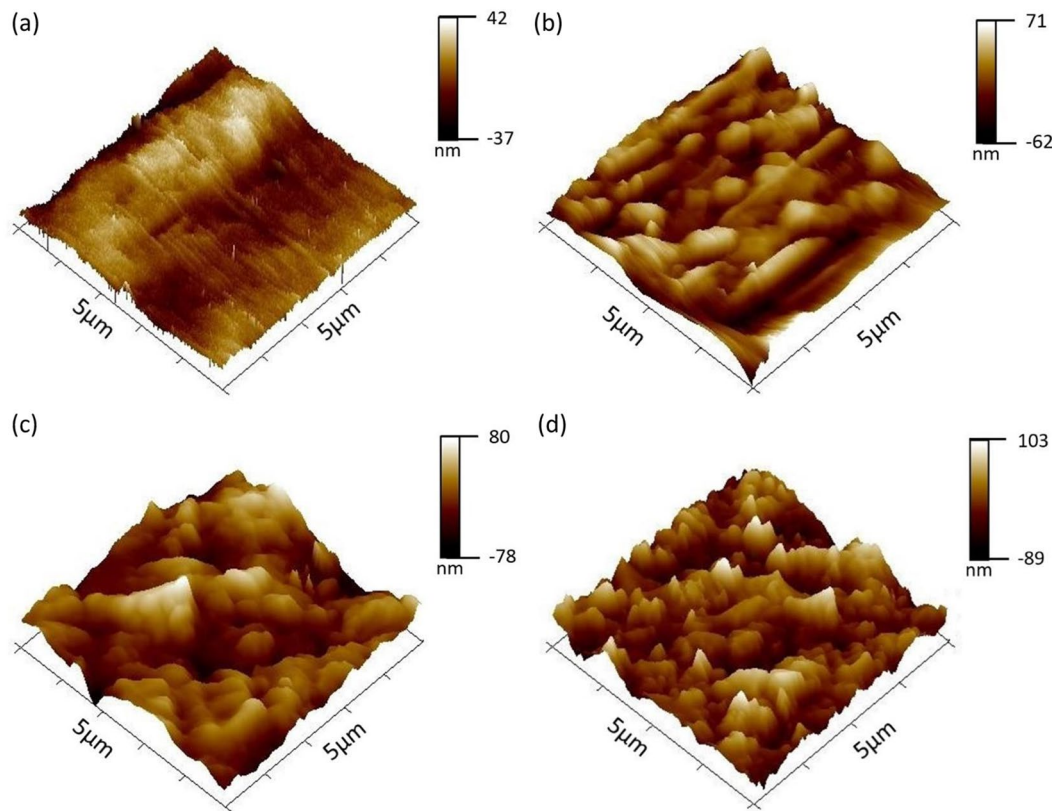


**Fig. 6** AFM images of various loading conditions of SS 316 L nano particles in resin matrix (a) Base resin, (b) 0.5%, (c) 1%, and (d) 1.5% SS 316 L

**Table 3** Regression coefficient values for nano-composite resin

Regression coefficients	Compression strength (MPa)	Specific wear rate ( $\text{mm}^3/\text{Nm}$ )
Intercept	160.69	0.5582
A-Reinforcement material	3.50	-0.0385
B-Stirring speed	2.50	-0.0035
C-Sonication time	4.50	-0.0115
AB	2.25	-0.0037
AC	1.25	-0.0008
BC	0.25	-0.0047
A <sup>2</sup>	-19.29	0.0296
B <sup>2</sup>	-1.29	0.0006
C <sup>2</sup>	-0.2941	-0.0074
<b>R<sup>2</sup></b>	<b>0.9907</b>	<b>0.9685</b>

variables, suggesting that the model is statistically accurate in representing the data.

Tables 4 and 5 illustrate the ANOVA test for compression strength and the wear test respectively. In case of compression strength, the F-value of the models is 166.29 that indicates that the model is significant with only a 0.01% chance it's due to noise. The model terms with p-values less than 0.05, such as A, B, C are significant. The Lack of Fit F-value of 0.09 shows that the lack of fit is not significant compared

to the pure error, with a 77.76% chance that such a high Lack of Fit F-value is due to noise. This is favorable for well fit of model. While, in case of specific wear rate, the F-value of the model is 48.80 indicates it is significant, with only a 0.02% chance it's due to noise. Significant model terms (p-values < 0.0500) include A, C, and A<sup>2</sup>. The Lack of Fit F-value of 0.93 suggests the model fits well, with a 39.05% chance the high value is due to noise, indicating non-significant lack of fit.

### 3.5 Effect of process parameters on responses

The compression strength of composite resin is dependent on the amount of reinforcement material due to its significant effect at linear, quadratic, and interaction levels with sonication time and stirring speed with  $p < 0.05$  for all factors. The other factors which also affected the compression strength slightly, were the linear and interactive terms of stirring speed and sonication time. Overall, Fig. 7 (a), (b), and (c) illustrates the relationship between the independent variables (sonication time, stirring speed, and reinforcement material) and the dependent variable (compression strength), allowing us to visually understand how these factors affect the compression strength of the composite resin. The observations indicate that the compression strength

**Table 4** ANOVA test for compression strength

Source	Sum of squares	df	Mean square	F-value	<i>p</i> -value	
<b>Model</b>	1592.01	9	176.89	166.29	<0.0001	significant
A-Reinforcement Material	24.50	1	24.50	23.03	0.0049	
B-Stirring Speed	12.50	1	12.50	11.75	0.0187	
C-Sonication time	40.50	1	40.50	38.07	0.0016	
AB	6.75	1	6.75	6.35	0.0532	
AC	2.08	1	2.08	1.96	0.2206	
BC	0.0833	1	0.0833	0.0783	0.7908	
A <sup>2</sup>	973.61	1	973.61	915.28	<0.0001	
B <sup>2</sup>	4.38	1	4.38	4.12	0.0982	
C <sup>2</sup>	0.2262	1	0.2262	0.2127	0.6640	
<b>Residual</b>	5.32	5	1.06			
Lack of Fit	0.1186	1	0.1186	0.0913	0.7776	not significant
Pure Error	5.20	4	1.30			
<b>Cor Total</b>	1597.33	14				

**Table 5** ANOVA test for specific wear rate

Source	Sum of squares	df	Mean square	F-value	<i>p</i> -value	
<b>Model</b>	0.0137	9	0.0015	48.80	0.0002	significant
A-Reinforcement Material	0.0030	1	0.0030	94.93	0.0002	
B-Stirring Speed	0.0000	1	0.0000	0.7845	0.4163	
C-Sonication time	0.0003	1	0.0003	8.47	0.0334	
AB	0.0000	1	0.0000	0.6004	0.4735	
AC	7.500E-07	1	7.500E-07	0.0240	0.8829	
BC	0.0000	1	0.0000	0.9633	0.3714	
A <sup>2</sup>	0.0023	1	0.0023	73.61	0.0004	
B <sup>2</sup>	1.095E-06	1	1.095E-06	0.0351	0.8588	
C <sup>2</sup>	0.0001	1	0.0001	4.53	0.0866	
<b>Residual</b>	0.0002	5	0.0000			
Lack of Fit	0.0000	1	0.0000	0.9256	0.3905	not significant
Pure Error	0.0001	4	0.0000			
<b>Cor Total</b>	0.0139	14				

shows an increase when the reinforcement material is increased up to 1%. However, if the reinforcement is further increased, the compression strength begins to decrease. Additionally, a slight increase in the compression strength is observed with higher stirring speeds and longer sonication times. The unmodified resin displayed a compression strength of 118 MPa, while the highest compression strength of 165 MPa was observed at a stirring speed of 1100 rpm, sonication time of 30 min, and 1% reinforcement. This demonstrates a significant and favorable influence of the process parameters on the compression strength. Furthermore, all the modified samples showed a significant impact when compared to the unmodified sample.

The wear resistance of dental restoration is an important factor to consider when choosing a suitable material for a patient. Dental crowns are subjected to forces during chewing and biting, and their durability is crucial for long-term success. The wear resistance of a dental crown depends on the material used, proper design, and its placement. The wear resistance is calculated in terms of specific wear rate.

The unmodified resin exhibited specific wear rate of 0.728 mm<sup>3</sup>/Nm, while the lowest wear rate of 0.532 mm<sup>3</sup>/Nm was observed at an 800 rpm stirring speed, 30-minute sonication time, and 1.5% reinforcement. In concern to this PMMA composite dental resin, the amount of reinforcement material had a pronounced effect on specific wear rate at linear ( $p < 0.001$ ) and quadratic levels ( $p < 0.05$ ). Other factors which significantly affect the specific wear rate were sonication time, the interaction of reinforcement material with stirring speed, and sonication time. Figure 7 (d), (e), and (f) enable us to visually interpret the effects of the independent variables on the dependent variable, helping us to make conclusions about how sonication time, stirring speed, and reinforcement material affect the specific wear rate of the composite resin. The data demonstrates that the wear rate declines as the reinforcement material increases to 1.2% and an additional increase in the reinforcement material slightly increases it. This happens because, beyond a certain point, higher concentrations of reinforcement material can lead to agglomeration, forming weak spots that aren't well-bonded

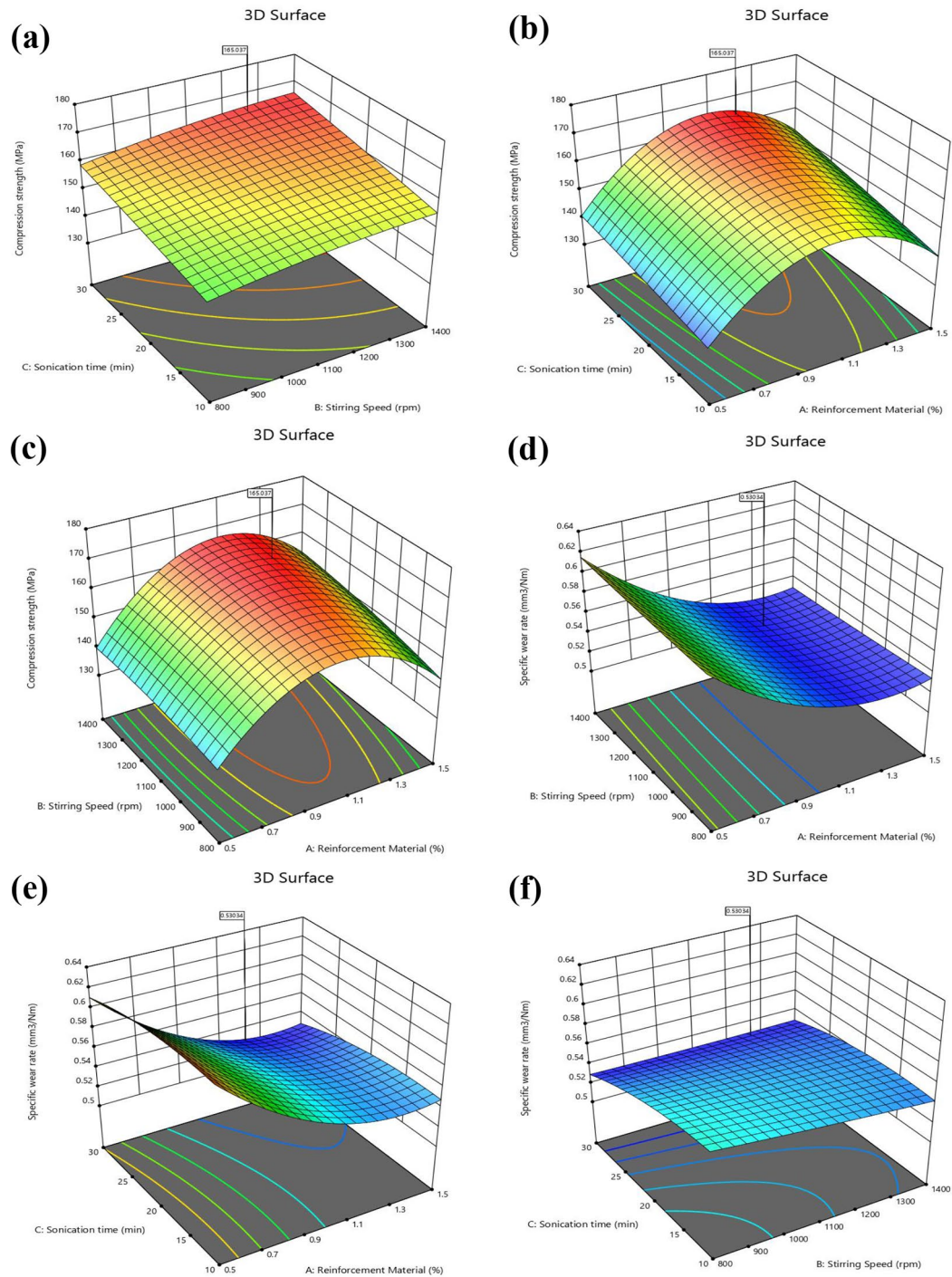


**Fig. 7** 3D graphic surface optimization of **(a)** Compression strength versus sonication time and stirring speed; **(b)** Compression strength versus sonication time and reinforcement material; **(c)** Compression strength reinforcement material and stirring speed; **(d)** Specific wear

rate versus reinforcement material and stirring speed; **(e)** Specific wear rate versus sonication time and reinforcement material; and **(f)** Specific wear rate versus sonication time and stirring speed

to the matrix. These weak spots can cause micro-fractures and higher wear. Additionally, excessive reinforcement can disrupt the material's structure, resulting in less efficient load distribution and increased wear. Moreover, the specific

wear rate is significantly affected by sonication time with  $p$ -value 0.033 which is less than 0.05, making it a significant model term, while minimally affected by the stirring speed. The specific wear rate decreases with increasing sonication

**Table 6** Requirement for multiple-objective optimization

Name	Goal	Lower Limit	Upper Limit	Lower Weight	Upper Weight	Importance
A: Reinforcement material	within limits	0.5	1.5	1	1	***
B: Stirring speed	within limits	800	140	1	1	***
C: Sonication time	within limits	10	30	1	1	***
Compression strength	maximize	133	165	1	1	***
Specific wear rate	minimize	0.532	0.634	1	1	***

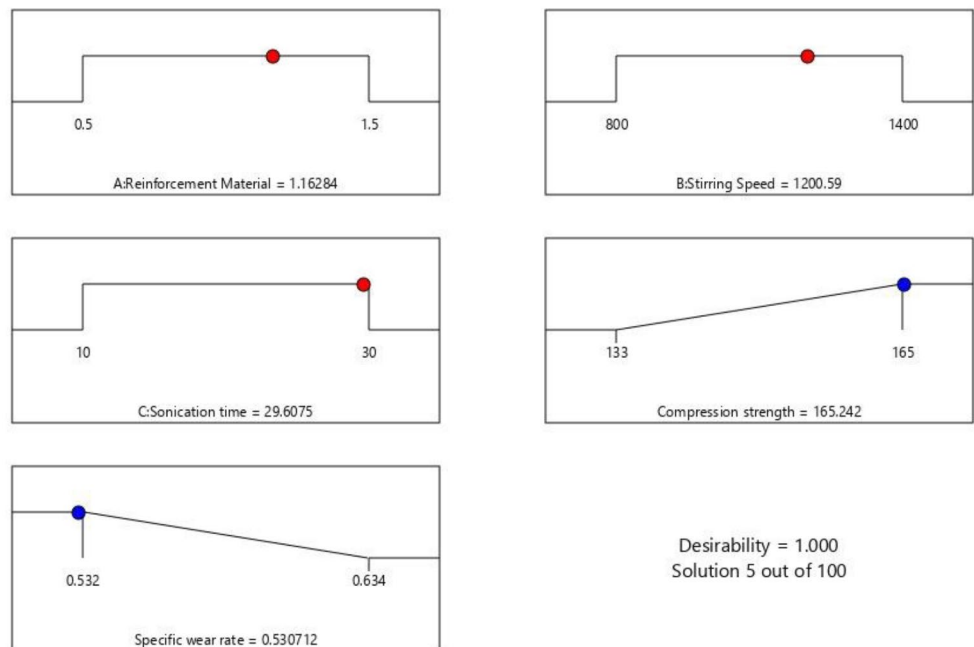
time because longer sonication improves the dispersion of nanoparticles and enhances their bonding with the matrix. These findings demonstrate a significant influence of the process parameters on the specific wear rate.

Further research can be done on the composite material by increasing the granularity of the reinforcement increments by 0.1%, which would indeed provide a more detailed understanding of the relationship between reinforcement material and mechanical properties. This approach would allow for a more precise analysis of the relationship among factors and responses, potentially revealing trends or patterns that may not be evident with larger increments. By identifying these finer details, researchers can gain deeper insights into the optimal range of reinforcement percentages for achieving desired mechanical properties in composite resin. By expanding the range of reinforcement increments, researchers can further refine their understanding of the relationship and make more informed decisions in designing and developing more effective and durable composite materials.

### 3.6 Optimization of process parameters

In this study, the process factors were optimized by implementing RSM (Response Surface Methodology). The primary objective was to enhance the compression strength while simultaneously decreasing the specific wear rate. To achieve this, a multi-objective optimization approach was employed to determine the optimal combination of process parameters that would yield the best outcomes. The specific requirements for the multi-objective optimization, including the responses, compression strength, and specific wear rate, are provided in Table 6. The results are displayed in the ramp graph in Fig. 8. The optimum process parameters – reinforcement material, stirring speed, and the sonication time - found to be 1.162% (w/w), 1200.59 rpm, and 29.6075 min, respectively, were needed to achieve the maximum compression strength and minimum specific wear rate simultaneously. The predicted compression strength and specific wear rate values are 165.242 MPa and 0.530712 mm<sup>3</sup>/Nm, respectively, at the optimal set of parameters.

**Fig. 8** Ramp function graphs for Multiple-objective optimization represent input independent factors' values and responses at optimized state with maximum desirability



### 3.7 Validation of results

The model was validated using the best possible process parameter combination revealed by the RSM-generated models at maximum desirability. To verify the accuracy of the projected models, a minimum of three specimens have been made using the best process parameter combination chosen for each magnitude. It is confirmed that the generated RSM model is adequate when the observed average minimum 0.12026% variation in compression strength and 0.05321% variation in specific wear rate was near the expected values of 0.15321% and 0.05932%, respectively.

## 4 Conclusion

The study introduced a successful development of a 3D printable nanocomposite with SS 316 L nano-fillers and PMMA resin and optimized its preparation conditions in order to minimize its specific wear rate and maximize its compressive strength using a Central Composite Design (CCD) approach in Response Surface Methodology (RSM). The major findings of the study are as follows:

- The incorporation of SS 316 L nanoparticles significantly enhanced both compression strength and wear resistance compared to unmodified resin material.
- Scanning Electron Microscopy (SEM) analysis revealed homogeneous dispersion of nanoparticles with some agglomeration observed at higher concentrations, resulting in lower compression strength at higher concentrations.
- The maximum experimental compression strength of 165 MPa was achieved at 1% SS 316 L nano-filler content, while the minimum specific wear rate of 0.532 mm<sup>3</sup>/Nm was observed at 1.5% filler content.
- The derived quadratic models accurately described and predicted the compression strength and wear resistance of the nanocomposite resin under varying preparation conditions (nano-filler content, stirring speed, and sonication time). The optimized conditions identified through RSM are as follows: 1.16% (w/w) SS 316 L nano-filler content, a stirring speed of 1200 rpm, and a sonication time of 29.6 min, resulting in predicted compression strength and specific wear rate values of 165.242 MPa and 0.530712 mm<sup>3</sup>/Nm, respectively.
- Experimental validation closely matched these predictions, confirming the reliability and precision of the RSM model for optimizing nanocomposite resin preparation.
- The results of this study hold great significance in the fabrication process of long-term provisional dental crowns and bridges.

**Acknowledgements** The author(s) duly acknowledges D.C.R.U.S.T., Murthal, Haryana for providing 3D printing and infrastructural facilities.

**Author contributions** Upender Punia: Methodology, Software, Validation, Writing – original draft. Ramesh Kumar Garg: Supervision, Data curation, Writing – review & editing.

**Data availability** Data will be made available on request.

### Declarations

**Competing interests** The author(s) declare that they have no known competing financial interests or personal relationships that could have appeared to influence the work reported in this paper.

## References

1. Zhou, J., Camba, J.D.: Computer-aided process planning in immersive environments: A critical review. *Comput. Ind.* **133**, 103547 (2021). <https://doi.org/10.1016/j.compind.2021.103547>
2. Gao, W., Zhang, Y., Ramanujan, D., Ramani, K., Chen, Y., Williams, C.B., Wang, C.C.L., Shin, Y.C., Zhang, S., Zavattieri, P.D.: The status, challenges, and future of additive manufacturing in engineering. *CAD Comput. Aided Des.* **69**, 65–89 (2015). <https://doi.org/10.1016/j.cad.2015.04.001>
3. Zhang, J., Xie, S., Li, T., Liu, Z., Zheng, S., Zhou, H.: A study of multi-stage energy absorption characteristics of hybrid sheet TPMS lattices. *Thin-Walled Struct.* **190**, 110989 (2023). <https://doi.org/10.1016/j.tws.2023.110989>
4. Jandyal, A., Chaturvedi, I., Wazir, I., Raina, A., Ul Haq, M.I.: 3D printing – a review of processes, materials and applications in industry 4.0. *Sustain. Oper. Comput.* **3**, 33–42 (2022). <https://doi.org/10.1016/j.susoc.2021.09.004>
5. Gernandt, S., Tomasella, O., Scolozzi, P., Felon, M.: Contribution of 3D printing for the surgical management of jaws cysts and benign tumors: A systematic review of the literature. *J. Stomatol. Oral Maxillofac. Surg.* **124**, 101433 (2023). <https://doi.org/10.1016/j.jormas.2023.101433>
6. R.D.B., D.D.: A review on Additive Manufacturing techniques in Medical Applications. *Int. J. Adv. Sci. Eng.* **5**, 988–997 (2019). <https://doi.org/10.29294/ijase.5.3.2019.988-997>
7. Tian, Y., Chen, C.X., Xu, X., Wang, J., Hou, X., Li, K., Lu, X., Shi, H.Y., Lee, E.S., Jiang, H.B.: A Review of 3D Printing in Dentistry. *Technologies, Affecting Factors, and Applications* (2021)
8. Polesel, A.: Restoration of the endodontically treated posterior tooth. *G Ital. Endod.* **28**, 2–16 (2014). <https://doi.org/10.1016/j.gien.2014.05.007>
9. Daher, R., Ardu, S., di Bella, E., Krejci, I., Duc, O.: Efficiency of 3D-printed composite resin restorations compared with subtractive materials: Evaluation of fatigue behavior, cost, and time of production. *J. Prosthet. Dent.* 1–8 (2022). <https://doi.org/10.1016/j.prosdent.2022.08.001>
10. Punia, U., Kaushik, A., Garg, R.K., Chhabra, D., Sharma, A.: 3D printable biomaterials for dental restoration: A systematic review. *Mater. Today Proc.* **63**, 566–572 (2022). <https://doi.org/10.1016/j.matpr.2022.04.018>
11. Aminoroaya, A., Neisiany, R.E., Khorasani, S.N., Panahi, P., Das, O., Madry, H., Cucchiari, M., Ramakrishna, S.: A review of dental composites: Challenges, chemistry aspects, filler influences, and future insights. *Compos. Part. B Eng.* **216**, 108852 (2021). <https://doi.org/10.1016/j.compositesb.2021.108852>

12. Chan, F.T.S., Lau, H.C.W., Ip, R.W.L., Chan, H.K., Kong, S.: Implementation of total productive maintenance: A case study. *Int. J. Prod. Econ.* **95**, 71–94 (2005). <https://doi.org/10.1016/j.ijpe.2003.10.021>
13. Balla, V.K., Kate, K.H., Satyavolu, J., Singh, P., Tadimetri, J.G.D.: Additive manufacturing of natural fiber reinforced polymer composites: Processing and prospects. *Compos. Part. B Eng.* **174**, 106956 (2019). <https://doi.org/10.1016/j.compositesb.2019.106956>
14. Zafar, M.S.: Prosthodontic applications of polymethyl methacrylate (PMMA): An update. *Polymers (Basel)*. **12**, 1–35 (2020). <https://doi.org/10.3390/polym12102299>
15. Lohbauer, U.: Dental glass ionomer cements as permanent filling materials? -Properties, limitations and future trends. *Mater. (Basel)*. **3**, 76–96 (2010). <https://doi.org/10.3390/ma3010076>
16. Somani, M.V., Khandelwal, M., Punia, V., Sharma, V.: The effect of incorporating various reinforcement materials on flexural strength and impact strength of polymethylmethacrylate: A meta-analysis. *J. Indian Prosthodont. Soc.* **19**, 101–112 (2019). [https://doi.org/10.4103/jips.jips\\_313\\_18](https://doi.org/10.4103/jips.jips_313_18)
17. Jandt, K.D., Watts, D.C.: Nanotechnology in dentistry: Present and future perspectives on dental nanomaterials. *Dent. Mater.* **36**, 1365–1378 (2020). <https://doi.org/10.1016/j.dental.2020.08.006>
18. Kumar, A., Sharma, K., Dixit, A.R.: A review of the mechanical and thermal properties of graphene and its hybrid polymer nanocomposites for structural applications. *J. Mater. Sci.* **54**, 5992–6026 (2019). <https://doi.org/10.1007/s10853-018-03244-3>
19. Korayem, A.H., Tourani, N., Zakertabrizi, M., Sabziparvar, A.M., Duan, W.H.: A review of dispersion of nanoparticles in cementitious matrices: Nanoparticle geometry perspective. *Constr. Build. Mater.* **153**, 346–357 (2017). <https://doi.org/10.1016/j.conbuildmat.2017.06.164>
20. Phogat, A., Chhabra, D., Sindhu, V., Ahlawat, A.: Analysis of wear assessment of FDM printed specimens with PLA, multi-material and ABS via hybrid algorithms. *Mater. Today Proc.* **62**, 37–43 (2022). <https://doi.org/10.1016/j.matpr.2022.01.429>
21. Yadav, R., Lee, H., Lee, J.H., Singh, R.K., Lee, H.H.: A comprehensive review: Physical, mechanical, and tribological characterization of dental resin composite materials. *Tribol Int.* **179**, 108102 (2023). <https://doi.org/10.1016/j.triboint.2022.108102>
22. Khmich, A., Hassani, A., Sbiaai, K., Hasnaoui, A.: Tuning of mechanical properties of Tantalum-based metallic glasses. *Int. J. Mech. Sci.* **204**, 106546 (2021). <https://doi.org/10.1016/j.ijmecsci.2021.106546>
23. Ahlawat, A., Phogat, A., Yadav, M., Sahdev, R.K., Dhingra, A.K., Chhabra, D.: Fabrication and analysis of ABS-HDPE-PC composite polymer filament used for FDM printing using hybrid algorithm. *Int. J. Interact. Des. Manuf.* **17**, 3199–3209 (2023). <https://doi.org/10.1007/s12008-023-01389-3>
24. Pande, S., Chaudhary, A., Patel, D., Singh, B.P., Mathur, R.B.: Mechanical and electrical properties of multiwall carbon nanotube/polycarbonate composites for electrostatic discharge and electromagnetic interference shielding applications. *RSC Adv.* **4**, 13839–13849 (2014). <https://doi.org/10.1039/c3ra47387b>
25. AlGhamdi, M.A., Alatiyyah, F.M., Dawood, Z.H.A., Alshaikhnasser, F.Y., Almedarham, R.F., Alboryh, S.Y., Elakel, A., Akhtar, S., Khan, S.Q., Gad, M.M.: Flexural strength of 3D-printed nanocomposite provisional resins: Impact of SiO<sub>2</sub> and ZrO<sub>2</sub> nanoparticles and printing orientations in vitro. *J. Prosthodont.* (2024). <https://doi.org/10.1111/jopr.13829>
26. AlGhamdi, M.A., Alatiyyah, F.M., Almedarham, R.F., Dawood, A., Alshaikhnasser, Z.H., Alboryh, F.Y., Khan, S.Y., Abualsaud, S.Q., Gad, R.: M.M.: Impact of Nanoparticle Addition on the Surface and Color Properties of Three-Dimensional (3D) Printed Polymer-Based Provisional Restorations. *Nanomaterials*. **14**, (2024). <https://doi.org/10.3390/nano14080665>
27. Yu, L., Zhu, Y., Wu, Q., Zhou, L., Wu, X., Zhang, Y., Zhou, J., Wang, Z.: 3D Printing of Zirconia Nanoparticle/Boron Nitride Nanosheet Multidimensional Reinforced Acrylic Matrix composites for Self-Lubricating materials. *ACS Appl. Nano Mater.* **6**, 21532–21547 (2023). <https://doi.org/10.1021/acsanm.3c03265>
28. Aati, S., Akram, Z., Ngo, H., Fawzy, A.S.: Development of 3D printed resin reinforced with modified ZrO<sub>2</sub> nanoparticles for long-term provisional dental restorations. *Dent. Mater.* **37**, e360–e374 (2021). <https://doi.org/10.1016/j.dental.2021.02.010>
29. Kuffner, B.H.B., Capellato, P., Ribeiro, L.M.S., Sachs, D., Silva, G.: Production and characterization of a 316l stainless steel/β-tcp biocomposite using the functionally graded materials (Fgms) technique for dental and orthopedic applications. *Met. (Basel)*. **11** (2021). <https://doi.org/10.3390/met11121923>
30. Arieira, A., Madeira, S., Rodrigues, F., Silva, F.: Tribological Behavior of TiO<sub>2</sub> PEEK Composite and Stainless Steel for Pediatric Crowns. *Mater. (Basel)*. **16** (2023). <https://doi.org/10.3390/ma16062420>
31. Gnanavel, S., Ponnusamy, S., Mohan, L., Muthamizhchelvan, C.: In Vitro Corrosion Behaviour of Ti–6Al–4V and 316L Stainless Steel alloys for Biomedical Implant Applications. *J. Bio- Tribo-Corrosion*. **4**, 1 (2018). <https://doi.org/10.1007/s40735-017-0118-8>
32. Hayes, A., Sharifi, S., Stack, M.M.: Micro-abrasion-corrosion maps of 316L Stainless Steel in Artificial Saliva. *J. Bio-Tribo-Corrosion*. **1**, 1–15 (2015). <https://doi.org/10.1007/s40735-015-0015-y>
33. Attar, H., Ehtemam-Haghighi, S., Soro, N., Kent, D., Dargusch, M.S.: Additive manufacturing of low-cost porous titanium-based composites for biomedical applications: Advantages, challenges and opinion for future development. *J. Alloys Compd.* **827**, 154263 (2020). <https://doi.org/10.1016/j.jallcom.2020.154263>
34. Toderăşcu, G., Dumitraşcu, V., Benea, L., Chiriac, A.: Corrosion Behaviour and Biocompatibility of 316 Stainless Steel as Biomaterial in physiological environment. 16–22 (2015)
35. Montazeri, A., Chitsazzadeh, M.: Effect of sonication parameters on the mechanical properties of multi-walled carbon nanotube/epoxy composites. *Mater. Des.* **56**, 500–508 (2014). <https://doi.org/10.1016/j.matdes.2013.11.013>
36. Suave, J., Coelho, L.A.F., Amico, S.C., Pezzin, S.H.: Effect of sonication on thermo-mechanical properties of epoxy nanocomposites with carboxylated-SWNT. *Mater. Sci. Eng. A*. **509**, 57–62 (2009). <https://doi.org/10.1016/j.msea.2009.01.036>
37. Montazeri, A., Montazeri, N., Pourshamsian, K., Tcharkhtchi, A.: The effect of sonication time and dispersing medium on the mechanical properties of multiwalled carbon nanotube (MWCNT)/epoxy composite. *Int. J. Polym. Anal. Charact.* **16**, 465–476 (2011). <https://doi.org/10.1080/1023666X.2011.600517>
38. Shirmohammadi, M., Goushchi, S.J., Keshtiban, P.M.: Optimization of 3D printing process parameters to minimize surface roughness with hybrid artificial neural network model and particle swarm algorithm. *Prog Addit. Manuf.* **6**, 199–215 (2021). <https://doi.org/10.1007/s40964-021-00166-6>
39. Radhwan, H., Shayfull, Z., Farizuan, M.R., Effendi, M.S.M., Irfan, A.R.: Optimization parameter effects on the quality surface finish of the three-dimensional printing (3D-printing) fused deposition modeling (FDM) using RSM. *AIP Conf. Proc.* **2129**, (2019). <https://doi.org/10.1063/1.5118163>
40. El Magri, A., El Mabrouk, K., Vaudreuil, S., Ebn Touhami, M.: Experimental investigation and optimization of printing parameters of 3D printed polyphenylene sulfide through response surface methodology. *J. Appl. Polym. Sci.* **138** (2020). <https://doi.org/10.1002/app.49625>
41. Han, Y., Wang, F.K., Wang, H., Jiao, X., Chen, D.: High-strength boehmite-acrylate composites for 3D printing: Reinforced

- filler-matrix interactions. *Compos. Sci. Technol.* **154**, 104–109 (2018). <https://doi.org/10.1016/j.compscitech.2017.10.026>
42. AATI, S., Aneja, S., Kassara, M., Leung, R., Nguyen, A., Tran, S., Shrestha, B., Fawzy, A.: Silver-loaded mesoporous silica nanoparticles enhanced the mechanical and Antimicrobial properties of 3d printed denture base Resin. *SSRN Electron. J.* (2022). <https://doi.org/10.2139/ssrn.4166940>

Springer Nature or its licensor (e.g. a society or other partner) holds exclusive rights to this article under a publishing agreement with the author(s) or other rightsholder(s); author self-archiving of the accepted manuscript version of this article is solely governed by the terms of such publishing agreement and applicable law.

**Publisher's Note** Springer Nature remains neutral with regard to jurisdictional claims in published maps and institutional affiliations.